2014

Comparison of Upscaled Models for Multistage Mass Discharge from DNAPL Source Zones

Amalia Kokkinaki
University of San Francisco, akokkinaki@usfca.edu

C J. Werth

B E. Sleep

Recommended Citation
Kokkinaki, A., C. J. Werth, and B. E. Sleep (2014), Comparison of upscaled models for multistage mass discharge from DNAPL source zones, Water Resour. Res., 50, 3187–3205, http://dx.doi.org/10.1002/2013WR014663.

AGU PUBLICATIONS

Water Resources Research

RESEARCH ARTICLE
10.1002/2013WR014663

Key Points:
- A new upscaled relationship captures multistage DNAPL mass discharge
- Changes in three macroscopic source zone metrics control effluent concentrations
- Slope changes in concentration profiles were not related to ganglia depletion

Supporting Information:
- Readme
- Main supporting information file with text
- FIgure S1

Correspondence to:
B. E. Sleep,
sleep@ecf.utoronto.ca

Citation:
Kokkinaki, A., C. J. Werth, and B. E. Sleep (2014), Comparison of upscaled models for multistage mass discharge from DNAPL source zones, *Water Resour. Res.*, *50*, 3187–3205, doi:10.1002/2013WR014663.

Received 28 AUG 2013
Accepted 20 MAR 2014
Accepted article online 25 MAR 2014
Published online 10 APR 2014

Comparison of upscaled models for multistage mass discharge from DNAPL source zones

A. Kokkinaki[1], C. J. Werth[2], and B. E. Sleep[1]

[1]Department of Civil Engineering, University of Toronto, Toronto, Ontario, Canada, [2]Department of Civil and Environmental Engineering, University of Illinois at Urbana-Champaign, Urbana, Illinois, USA

Abstract Analytical upscaled models that can describe the depletion of dense nonaqueous phase liquids (DNAPLs) and the associated mass discharge are a practical alternative to computationally demanding and data-intensive multiphase numerical simulators. A major shortcoming of most existing upscaled models is that they cannot reproduce the nonmonotonic, multistage effluent concentrations often observed in experiments and numerical simulations. Upscaled models that can produce multistage concentrations either require calibration, which increases the cost of applying them in the field, or use dual-domain conceptual models that may not apply for spatially complex source zones. In this study, a new upscaled model is presented that can describe the nonmonotonic, multistage average concentrations emanating from complex DNAPL source zones. This is achieved by explicitly considering the temporal evolution of three source zone parameters, namely source zone projected area, the average of local-scale DNAPL saturations, and the average of local-scale aqueous relative permeability, without using empirical parameters. The model is evaluated for two real and twelve hypothetical centimeter-scale complex source zones. The proposed model captures the temporal variations in concentrations better than an empirical model and a dual-domain ganglia-to-pool ratio model. The results provide evidence that effluent concentrations downgradient of DNAPL source zones are controlled by the evolution of the aforementioned macroscopic parameters. This knowledge can be useful for the interpretation of field observations of effluent concentrations downstream of DNAPL source zones, and for the development of predictive upscaled models. Advances in DNAPL characterization techniques are needed to quantify these macroscopic parameters that can be used to guide DNAPL remediation efforts.

1. Introduction

The longevity of dense nonaqueous phase liquid (DNAPL) source zones and the associated mass discharge depend on complex and interdependent multiphase processes occurring at the local scale, and are strongly influenced by fine-scale soil heterogeneity [*Kueper et al*., 1989; *Gerhard and Kueper*, 2003b]. Multiphase numerical models can be used to predict these processes, but they require detailed knowledge of soil heterogeneity and DNAPL release conditions [*Grant and Gerhard*, 2007; *Kokkinaki et al*., 2013a]. Furthermore, the computational cost of such models is prohibitive for application to large-scale systems. These difficulties have motivated the search for simpler, upscaled models that capture the average response downgradient of DNAPL source zones, and that require a small set of parameters that can be measured in the field.

Upscaled models (sometimes referred to as macroscopic, effective, or field-scale models) are based on conceptualizing a multidimensional, possibly heterogeneous, domain as a one-dimensional homogeneous domain. Unlike discretized numerical models that require knowledge of soil properties for every numerical block at the local, representative elementary volume (REV) scale, upscaled models are simple analytical expressions solved at the much larger domain scale, and parameterized with domain-averaged parameters that control the total mass discharge. Such upscaled models can be used to calculate the average effluent concentration for an entire control plane perpendicular to the mean groundwater flow, located downgradient from the DNAPL source zone, and from that, the expected longevity of the source zone. These domain-averaged analytical upscaled models are different from numerical models that solve the flow and transport equations in coarsely discretized domains using effective (sometime also called upscaled) variables for each grid block of the domain, and that are specific to the discretization chosen. Domain-averaged analytical models involve no discretization and describe the domain as a whole, irrespective of its size.

In order to develop analytical upscaled models (hereafter upscaled models), research efforts have focused on identifying relationships to describe the aggregate effect of the temporally and spatially complex DNAPL source zones on total mass discharge. Several studies have proposed that power law relationships can be used to link the effluent concentrations to the DNAPL mass remaining in the system [*Zhu and Sykes*, 2004; *Falta et al*., 2005a, 2005b]:

$$\frac{\bar{C}_L(t)}{\bar{C}_0} = \left(\frac{M(t)}{M_0}\right)^{\Gamma} \tag{1}$$

where $\bar{C}_L$ is the flux-averaged concentration at a control plane at a distance L from the source zone at time t, $\bar{C}_0$ is the flux-averaged concentration at the control plane that corresponds to the initial DNAPL mass M_0, $M(t)$ is the DNAPL mass remaining at time t, and Γ is an empirically determined or calibrated constant.

Another type of model that has been used to upscale DNAPL dissolution is the equilibrium streamtube method, which is based on a Lagrangian description of travel times and DNAPL saturations. The streamtube method relates concentration reductions to a source depletion term, S_D [*Jawitz et al*., 2003, 2005; *Basu et al*., 2008b]:

$$\frac{\bar{C}_L(t)}{f_c C_{eq}} = 1 - S_D(t) \tag{2}$$

where C_{eq} is the DNAPL solubility, and $f_c = \bar{C}_0 / C_{eq}$. The term S_D is the cumulative distribution function of the reactive travel time τ, which is a joint statistical distribution of organic saturation and time. Being a statistical distribution, S_D is parameterized by the mean, $\mu_{ln\tau}$, and the standard deviation, $\sigma_{ln\tau}$, of the log-transformed reactive travel time. The values of these parameters can be obtained by partitioning and nonpartitioning tracer tests conducted in the DNAPL region.

A third type of upscaled models is based on combining the one-dimensional advection-dominated transport equation with an upscaled effective mass transfer coefficient, k_{eff}. In contrast to local mass transfer coefficients [e.g., *Saba and Illangasekare*, 2000; *Nambi and Powers*, 2003], k_{eff} incorporates the domain-averaged effects of system size, soil heterogeneity, flow bypassing, and dilution. k_{eff}-type models (also called effective Damköhler number models) calculate effluent concentrations using the analytical solution of the advection-dissolution transport equation at steady state [*Parker and Park*, 2004]:

$$\frac{\bar{C}(L)}{C_{eq}} = 1 - exp\left(-\frac{k_{eff} L}{\bar{q}}\right) \tag{3}$$

where $\bar{q}$ is the average Darcy velocity of an equivalent one-dimensional, uniform flow field. The term k_{eff} is the controlling parameter of equation (3), capturing the average behavior of the spatially and temporally variable source zone architecture. Typically, k_{eff} is related to DNAPL and system properties through a power law model with one or more constant coefficients β [*Parker and Park*, 2004; *Christ et al*., 2006; *Saenton and Illangasekare*, 2007].

The underlying hypothesis of all three types of upscaled models described above is that the attributes of a source zone that control the changes in effluent concentrations with time are captured by the constant coefficients Γ, $\sigma_{ln\tau}$, and β. Calibration of these coefficients has been successfully used to fit concentrations downstream of simulated DNAPL source zones, and has shown that they are related to the source zone architecture. In the case of the streamtube model, this relation to the source zone architecture is explicit in the definition of the reactive travel time, rather than empirical. These source zone-related coefficients control the decrease rate of the smooth, monotonically decreasing exponential functions that all three models produce.

However, source zone architectures that are complex, such as those encountered in heterogeneous aquifers, often result in nonsmooth effluent concentrations profiles with multiple stages and with slopes that abruptly increase and decrease in time as the source is being depleted (e.g., Figure 1). This is likely a result

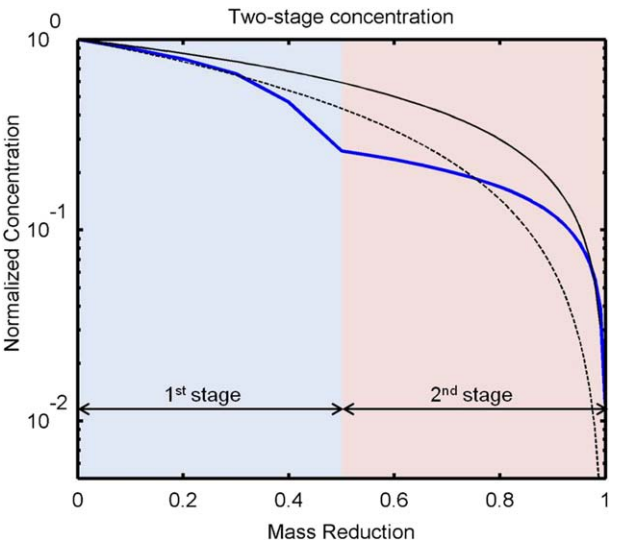

Figure 1. Idealized schematic of concentrations exhibiting a two-stage behavior, characteristic of source zones with complex architectures. Black lines show the implications of using power law models to fit early (dashed line) and late (solid line) time data.

of considerable changes in the source zone architecture as dissolution progresses [*Parker and Park*, 2004; *Basu et al*., 2008a; *Christ et al*., 2010]. This behavior has been observed in the field [*Brusseau et al*., 2007], in laboratory experiments [*Suchomel and Pennell*, 2006; *Zhang et al*., 2008; *DiFilippo et al*., 2010], and in numerical simulations [*Parker and Park*, 2004; *Falta et al*., 2005b; *Christ et al*., 2006, 2010; *Lemke and Abriola*, 2006; *Fure et al*., 2006; *Basu et al*., 2008b]. Understanding the underlying causes of this complex evolution of effluent concentrations is crucial, because it determines the overall source zone longevity, and, thus, may complicate remediation efforts if not properly accounted for [*SERDP*, 2006]. In addition, concentration reductions are important as performance metrics for risk-based management of DNAPL sites [*Rao et al*., 2002; *ITRC*, 2004, 2010]. Knowledge of the factors and DNAPL architectures that lead to such reductions can also help evaluate the conditions under which partial source removal is beneficial, and improve our overall ability to predict the outcome of remediation [*U.S. EPA*, 2003; *SERDP*, 2006].

Such complex multistage concentration profiles cannot be captured by the three types of upscaled models described previously. Applying such models for source zones that exhibit multistage concentration profiles will inevitably under or overpredict concentrations for parts of the source zone lifetime, as the smooth predicted concentration profile cannot match the entire breakthrough curve (Figure 1). Calibrating the coefficients continually can be used to provide better fits, but it does not improve the ability of the model to explain or to predict the observed behavior. To predict multistage concentrations without calibration, upscaled models need to include parameters that control the temporal changes in source zone architecture. Two different approaches have been proposed in the literature to achieve this, both based on the k_{eff}-type upscaled model (equation (3)).

The first approach is based on conceptualizing DNAPL source zones as dual-domain systems. By assigning a different exponent β for each domain, two-stage mass discharge can be reproduced. *Christ et al*. [2010] presented the first formal dual-domain upscaled model, by extending the *Christ et al*. [2006] ganglia-to-pool (GTP) model that was for ganglia-dominated sources. In the dual-domain GTP model, each of the two-domains (ganglia dominated and pool dominated) is associated with a mass reduction term, and a different, but constant, exponent β. The onset of the second stage of concentrations is related to the complete depletion of ganglia and the predominance of DNAPL pools.

The second approach that has been used to predict multistage concentrations is based on relating effluent concentrations to transient variables directly linked to source zone characteristics, which are updated as they change in time. *Saenton and Illangasekare* [2007] conducted a numerical study where they developed a power law correlation between k_{eff} and the second spatial moment of the DNAPL distribution. By considering transient spatial attributes of the source zone, they explicitly accounted for changes in the source zone architecture over time. Such changes can be both nonmonotonic and multistaged, in contrast to the exponentiated mass reduction term of *Christ et al*. [2010], which is a smooth, monotonically decreasing function.

In this paper, a new approach is presented which is based on a process-based conceptualization of k_{eff}. The process-based (PB) upscaled model is compared to the *Christ et al*. [2010] and the *Saenton and Illangasekare* [2007] upscaled models, and the models are evaluated for their ability to reproduce nonmonotonic,

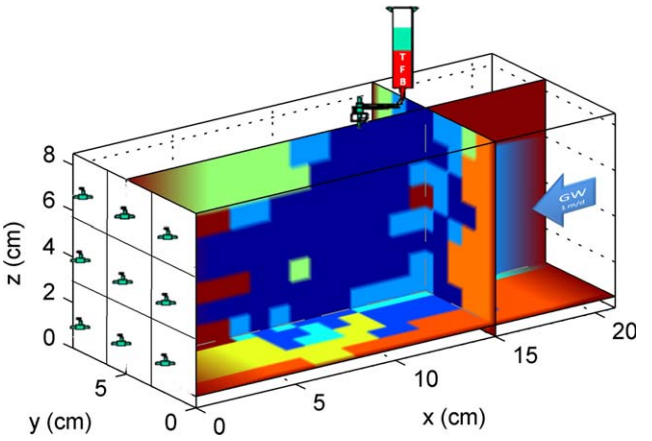

Figure 2. Schematic of the domain evaluated in all simulations. The soil type definition shown corresponds to Experiment 1 of *Zhang et al*. [2008]. Soil type definition, DNAPL amount, hydraulic gradient, and point of injection were varied for the hypothetical source zones.

multistage concentrations resulting from the dissolution of a range of complex centimeter-scale DNAPL source zones. Models of the power law type and streamtube models are not evaluated in detail here because they cannot produce multistage concentrations. For the evaluation of the upscaled models, DNAPL source zones are generated from a finely discretized multiphase numerical model using a thermodynamic dissolution model for local-scale DNAPL dissolution, which explicitly considers DNAPL-water interfacial areas and that was validated in previous work [*Kokkinaki et al*., 2013a, 2013b]. Here the evaluation of the upscaled models is performed using two source zones based on experiments from *Zhang et al*. [2007, 2008], and 12 additional hypothetical source zones created by changing key system conditions of these experiments. The proposed PB model is shown to effectively reproduce the nonmonotonic, multistage concentrations emanating from all DNAPL source zones, despite their significantly different source zone architectures.

2. Methods

2.1. Systems Investigated

The DNAPL dissolution experiments of *Zhang et al*. [2007, 2008] (Experiments 1 and 2) were conducted in two three-dimensional flow cells ($21 \times 8.8 \times 8.5$ cm^3), each packed with a different spatially correlated random permeability field (Figure 2). 22.5 mL of the single-species DNAPL 1,3,5-trifluorobenzene were released on the surface of each experimental cell and were allowed to equilibrate, resulting in an irregularly distributed source zone, that was subsequently flushed with water at a velocity of 1 m/d until the DNAPL was completely dissolved.

The DNAPL source zones of the two experiments were characterized by high-saturation pools with a complex architecture that caused significant flow bypassing and sharp changes in the source zone spatial distribution. This resulted in average effluent concentrations that exhibited a multistage, nonmonotonic behavior for both DNAPL source zones (Figure 3). Previous efforts to capture this complex mass discharge with upscaled dissolution models showed that models that do not consider the temporal evolution of the source zone architecture, including the equilibrium streamtube model of *Jawitz et al*. [2005], could not match experimental observations [*Zhang et al*., 2008]. Because of their complexity, the two source zones of these experiments were used as the first two test cases for the evaluation of the upscaled models discussed in the present study.

In addition to the DNAPL experiments of *Zhang et al*. [2007, 2008], 12 hypothetical cases of DNAPL dissolution were simulated with the discretized numerical model by varying system conditions (DNAPL amount, hydraulic gradient, soil type definition and point of injection), in order to produce a wider range of source zone architectures. The same centimeter -scale domain of the original experiments was used in all numerical simulations. The advantage of using centimeter-scale domains for this evaluation is that the numerical model can be finely discretized such that each grid block corresponds to the representative elementary volume (REV), where local-scale variables can be appropriately defined. This ensures that the numerical results are representative of the physical systems and can, therefore, provide an appropriate validation data set for the evaluation of the upscaled models. The use of centimeter-scale domains in this evaluation does not impact the generality of our conclusions, as all upscaled models discussed (equations 1–3) describe

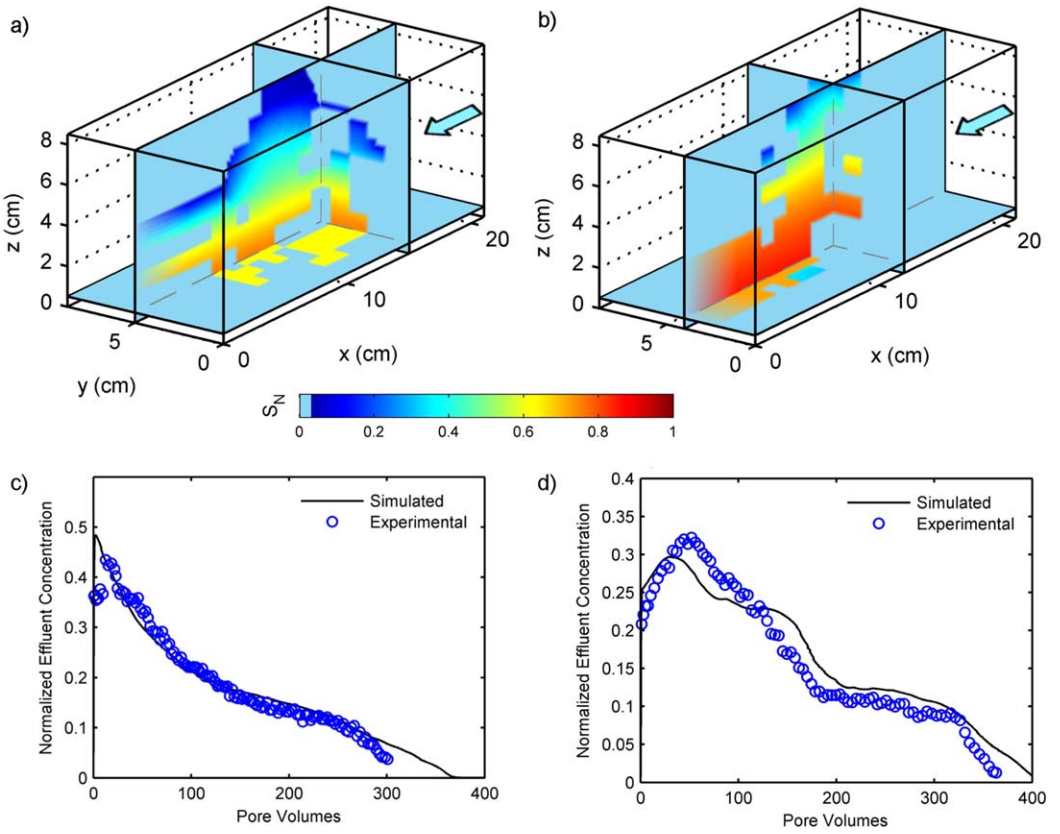

Figure 3. (a and b) DNAPL saturations at the end of the infiltration period and (c and d) normalized flux-averaged effluent concentrations predicted by COMPSIM and experimentally measured for (left) Experiment 1 and (right) Experiment 2.

domain-averaged quantities using one analytical equation which refers to the domain as a whole and that can be applied to domains beyond the centimeter scale.

2.2. Discretized Numerical Model

Finely discretized multiphase numerical simulations consider all relevant physical processes at the grid scale and use local (as opposed to effective or upscaled) mass transfer coefficients to simulate DNAPL dissolution. These simulations also explicitly consider the detailed source zone architecture, as well as its impact on the aqueous flow field. Provided that the discretization is close enough to the representative elementary volume (REV) of the simulated physical system, predictions by such discretized numerical models can provide appropriate validation data sets for the evaluation of upscaled models.

The numerical model used for this purpose in this study is COMPSIM, a three-dimensional, multicomponent, finite differences model that simulates multiphase flow and advective-dispersive transport in groundwater [*Sleep and Sykes*, 1993a, 1993b]. COMPSIM has been used in the literature to simulate groundwater contamination and remediation of organic compounds [*McClure and Sleep*, 1996; *Sleep et al*., 2000; *O'Carroll and Sleep*, 2007, 2009]. To simulate DNAPL infiltration, COMPSIM allows the use of infiltration models of varying complexity, from simple Brooks-Corey to the complex hysteretic constitutive relationships of *Gerhard and Kueper* [2003a, 2003c]. The latter relationships have been shown to result in more realistic DNAPL source zone architectures in heterogeneous domains [*Gerhard and Kueper*, 2003b], and for this reason they were utilized in the present study. A source/sink term is used to simulate kinetic mass transfer between phases. For mass transfer between the DNAPL and the aqueous phase, COMPSIM allows the use of a range of models, including a thermodynamic model and a number of empirical Sherwood-Gilland models. In this study, the thermodynamic model was utilized because, unlike empirical dissolution models, it is able to predict local dissolution rates for source zones of complex architecture without calibration [*Kokkinaki et al*., 2013a, 2013b].

In order to create the validation data set for the 14 DNAPL source zones and their associated concentration profiles, COMPSIM was used to predict the initial source zone architecture by simulating DNAPL infiltration in the heterogeneous domains, and the effluent concentrations by simulating DNAPL dissolution during the flushing period. For the two real experiments, the numerical data predicted by COMPSIM were used in place of experimental data because they provided a more detailed data set at later times of the experiments, and because they have been previously shown to represent well the observed concentrations and source zone architecture [*Kokkinaki et al*., 2013a]. For these simulations, the modeled permeability fields exactly matched the soil packing of the experimental flow cells, and soil properties were obtained from previous studies where the sands used were independently characterized [*Schroth et al*., 1996; *Dobson et al*., 2006; *Zhang et al*., 2008]. For the hypothetical simulations, attributes of the original experiments were varied to produce different source zone architectures. In all cases, the discretization of the domain (0.25 × 0.25 × (0.21–0.31) cm^3) was at the REV scale.

2.3. Upscaled Models

The upscaled models evaluated in this study belong to the category of the k_{eff} models (equation (3)), which is based on simplifying the governing equations for advective-dispersive transport and DNAPL dissolution in the three-dimensional space, to a simpler, one-dimensional upscaled equation. This simplification becomes possible under the following assumptions [*Parker and Park*, 2004; *Christ et al*., 2006]: (1) a one-dimensional uniform flow field with velocity $\bar{q}$ can reasonably approximate the flow field of the heterogeneous, three-dimensional system, (2) molecular diffusion and dispersion are negligible, (3) nonreactive conditions, (4) quasi-steady state dissolution kinetics, and (5) an effective, upscaled mass transfer rate (k_{eff}) can describe the cumulative mass transfer from the DNAPL source zone. Under these assumptions, flux-averaged concentrations, $\bar{C}$, at a distance x from the source are given by [*Parker and Park*, 2004; *Christ et al*., 2006]:

$$\bar{q}\left(\frac{d\bar{C}(x)}{dx}\right)=k_{eff}\left(C_{eq}-\bar{C}(x)\right) \tag{4}$$

Equation (4) can be analytically solved for a type I boundary condition at the upstream end of the domain $(\bar{C}(0)=0)$, and initial concentration of zero. Evaluated at distance L from the source zone, it results in equation (3). The term k_{eff} captures the integrated behavior of the spatially and temporally variable source zone architecture, and controls the temporal variations in the concentration profiles. The models that have been proposed to describe k_{eff} employ a power law function that can be generally expressed as:

$$k_{eff}(t)=k\prime_0\cdot M_{SZ,1}^{\beta_1}\cdot M_{SZ,2}^{\beta_2}\cdot\ldots=k'_0\cdot K_{SZ}(t) \tag{5}$$

The terms $M_{SZ,i}$ represent source zone metrics related to the DNAPL mass, system properties or source zone architecture, and β_i are fitting coefficients. The chosen metrics vary among different studies, and the coefficients depend on the specific source zones used for calibration of the models. The combined effect of these source zone metrics is represented here by the term $K_{SZ}(t)$, which encompasses the temporal changes in k_{eff}. The constant k'_0 represents the initial effective mass transfer rate, and its value is influenced by the extent of dilution, the scale of the system, and the size of the source zone. A practical way to obtain k'_0 is to use the observed initial concentration, $\overline{C}_0$ [*Christ et al*., 2006]. Combining equations (3) and (5) for $t=0$, and if K_{SZ} is defined such that $K_{SZ}(0)=1$, k'_0 is given by [*Christ et al*., 2006]:

$$k\prime_0=-\frac{\bar{q}}{L}ln\left(1-\frac{\overline{C_0}}{C_{eq}}\right) \tag{6}$$

Substituting equations (5) and (6) into equation (3) gives:

$$\frac{\bar{C}_L(t)}{C_{eq}}=1-\left(1-\frac{\overline{C_0}}{C_{eq}}\right)^{K_{SZ}(t)} \tag{7}$$

Equation (7) can be further simplified if the effective Damköhler number $k_{eff}L/\bar{q}$ is low [*Parker and Park*, 2004], or equivalently, if the initial concentration $\bar{C}_0$ is low. In this case, equation (7) converges to:

$$\frac{\bar{C}_L(t)}{C_{eq}} \approx \left(\frac{\overline{C_0}}{C_{eq}}\right) \cdot K_{SZ}(t) \tag{8}$$

For both equations (7) and (8), the term K_{SZ} is critical because it represents the source zone characteristics that control changes in the effluent concentrations with time. Next, three different approaches are discussed for calculating K_{SZ} representing three upscaled models that can produce multistaged effluent concentrations.

2.3.1. Dual-Domain GTP Model (DDGTP)

The dual-domain GTP model of *Christ et al*. [2010] is based on the commonly used description of k_{eff} as a function of the DNAPL mass remaining in the system [*Parker and Park*, 2004; *Christ et al*., 2006],

$$k_{eff} = k'_0 \cdot \left(\frac{M(t)}{M_0}\right)^{\beta} \tag{9}$$

such that K_{SZ} is given by equation (10):

$$K_{SZ}(t) = \left(\frac{M(t)}{M_0}\right)^{\beta} \tag{10}$$

Different values of the constant exponent β represent source zones of different characteristics. *Christ et al*. [2010] combined this approach with a dual-domain model that can reproduce two-stage concentration profiles. The source zone is conceptualized as the combination of a ganglia-dominated and a pool-dominated region, each being represented by a different β exponent. Employing equations (7) and (10) for each of the two-domains and summing the two terms gives the dual-domain GTP model (DDGTP) of *Christ et al*. [2010]:

$$\frac{\bar{C}_L(t)}{C_{eq}} = 2 - \left(1 - \frac{(1-f_x^p)\overline{C}_0}{C_{eq}}\right)^{\left(\frac{(1-PF(t))\cdot(M(t)/M_0)}{(1-PF_0)}\right)^{1.5}\left(\frac{1-PF_0}{PF_0}\right)^{-0.26}} - \left(1 - \frac{f_x^p \overline{C}_0}{C_{eq}}\right)^{\left(\frac{PF(t)\cdot(M(t)/M_0)}{PF_0}\right)^{0.5}} \tag{11}$$

where f_x^p is the proportion of mass flux attributable to pool dissolution and PF is the pool fraction of the source zone. The first term corresponds to dissolution from the ganglia-dominated part of the source zone, for which the exponent is given by an empirical relationship, and is a function of the initial pool fraction, PF_0 [*Christ et al*., 2006]. The second term of equation (11) corresponds to the dissolution from the pool-dominated region, for which a constant exponent equal to 0.5 is assumed. The contribution of each of the two terms is determined by the value of *PF*, which is assumed to increase as ganglia dissolve, until it reaches unity and pools dominate the source zone. An empirical relationship is used to calculate the increase of *PF* as a function of mass reduction [*Christ et al*., 2010]:

$$PF(t) = \begin{cases} 1-(1-PF_0)\left(1-\left(\dfrac{M(t)}{(1-PF_0)M_0}\right)^{(5.6\pm 2.6)}\right), \\ \qquad \text{if } \left(\dfrac{M(t)}{M_0}\right) \le (1-PF_0) \\ 1, \\ \qquad \text{otherwise} \end{cases} \tag{12}$$

The fundamental hypothesis of the DDGTP model is that the abrupt change in concentrations (second stage) is caused by the transition from a mixed, but ganglia-dominated source zone to a source zone comprising of DNAPL pools. The signal from the ganglia initially dominates that from pools, producing high initial effluent concentrations and low concentration reductions at the control plane (first stage). When mass reduction is equal to the initial ganglia fraction, $GF_0 = 1 - PF_0$ (i.e., all ganglia are depleted), concentrations

drop to the second stage. As such, the value of GF_0 is critical for the *Christ et al*. [2010] model, as it singularly determines the time for the beginning of the second stage of concentrations. The initial concentration of the second stage is determined by f_x^p.

Christ et al. [2010] showed that the dual-domain model is a reasonable approximation for hypothetical source zones created by combining a slow continuous DNAPL release and emplaced DNAPL pools. This architecture allows a clear transition from ganglia-to-pool dominance, as the DNAPL pools dissolve much slower than the ganglia. However, based on the DDGTP model, a second stage of concentrations would not occur in systems that were pool dominated initially. Also, the DDGTP model cannot produce effluent concentrations that exhibit more complex behavior, i.e., more than two-stages, or increasing concentrations. Overall, although the DDGTP model is unique because it only requires initial source zone characteristics to predict effluent concentrations (i.e., it is predictive), its applicability to more complex source zones needs to be further tested.

2.3.2. Empirical Spatial Moments Model (ESM)

Saenton and Illangasekare [2007] developed a model for upscaled mass transfer based on the hypothesis that the upscaled k_{eff} adheres to the same power law relationship that has been extensively used for local-scale mass transfer rates (i.e., Sherwood-Gilland models). *Saenton and Illangasekare* [2007] proposed that k_{eff} is correlated with the aquifer heterogeneity and the DNAPL architecture. Using a Monte Carlo analysis in two-dimensional domains, k_{eff} was given by the following empirical correlation:

$$k_{eff}(t)=k_0\left(1+\sigma_{lnk}^2\right)^{1.783}\left(1+\frac{\Delta_y}{\lambda_y}\right)^{2.35}\left(\frac{M_{ll,y}(t)}{M_{ll,y}^*}\right)^{4.157} \tag{13}$$

where k_0 is the local mass transfer coefficient, σ_{lnk}^2 is the variance of the log normally distributed intrinsic permeability, Δ_y is the vertical dimension of the upscaled domain, λ_y is the vertical correlation length, and $M_{ll,y}$ is the second spatial moment of the NAPL saturations in the vertical direction, which is normalized by its maximum value at the beginning of dissolution $\left(M_{ll,y}^*\right)$.

The original ESM model requires information on soil heterogeneity, as well as the value of k_0. While soil heterogeneity parameters may be known for a given domain, k_0 is typically defined at the local scale, and it can vary considerably throughout the source zone. The uncertainty associated with the value of k_0 can be easily circumvented as follows: for a given domain, all constant parameters of equation (13) can be lumped into a single constant, corresponding to k'_0 of equation (6), which can be determined by the initial concentration as previously described. Then, combining equations (5) and (13), the ESM model for K_{SZ} is obtained:

$$K_{SZ}(t)=\left(\frac{M_{ll,y(t)}}{M_{ll,y}^*}\right)^{\beta}, \text{where } \beta=4.157 \tag{14}$$

The main attribute of the *Saenton and Illangasekare* [2007] model is that $M_{ll,y}$ is updated as the source zone is changing with time. In this way, changes in the source zone architecture are explicitly considered, and nonmonotonic changes in K_{SZ} are possible, unlike with equation (11). However, a shortcoming of the ESM model is that it is a regression-based model and includes the empirical coefficient β, which needs to be calibrated for every different system the model is applied to. Here the ESM model (equation (14)) was evaluated using both the original and a calibrated coefficient β.

2.3.3. Process-Based (PB) Model

The third model evaluated is a new upscaled model that is based on identifying the physical processes that control concentration variations, and incorporating the relative temporal changes of metrics related to these processes in the upscaled mass transfer coefficient, k_{eff}. This approach leads to a process-based (PB) upscaled model. *Kokkinaki et al*. [2013a] showed that the factors controlling the effluent concentrations are the source zone extent and DNAPL dissolution kinetics. Based on this, the following representation of K_{SZ} is used here:

$$K_{SZ}(t) = \left(\frac{A_{yz,t}}{A_{yz,0}}\right) \cdot \left(\frac{\bar{k}_{wr,t}}{\bar{k}_{wr,0}}\right) \cdot \left(\frac{\bar{S}_{N,t}}{\bar{S}_{N,0}}\right) \quad (15)$$

$A_{yz,t}$ represents the projection of the source zone onto a control plane transverse to the flow direction, normalized by the total area of the control plane. This normalized area is the percentage of the control plane that is directly downgradient of the DNAPL source zone and captures the effect of dilution on effluent concentrations as the source zone is shrinking. In principle, $A_{yz,t}$ represents the cross-sectional extent of the source zone as a percentage of the control plane and is similar to the parameter f_x^p used in *Christ et al*. [2010], and the f_c term used in the streamtube model of *Jawitz et al*. [2005]. As $A_{yz,t}$ decreases with time relative to its initial value $A_{yz,0}$ due to dissolution, it results in an increase in the contribution of DNAPL-free water in the effluent, and a corresponding decrease in flux-averaged effluent concentrations.

$\bar{k}_{wr,t}$ and $\bar{S}_{N,t}$ represent the average of local water relative permeabilities and DNAPL saturations within the source zone, respectively, at a given time t. Water relative permeability and DNAPL saturation represent the well-established effects of velocity and interfacial area on the local mass transfer rates. Increases in relative permeability result in higher velocities and higher mass transfer rates, and to more flow through the source zone. Conversely, decreasing interfacial areas result in lower mass transfer rates. To incorporate these effects in the PB upscaled model, it is assumed that the source zone-averaged values of relative permeability and organic saturation capture the total effect of the critical local changes in mass transfer. Local water relative permeabilities are calculated by the Brooks-Corey model and arithmetic averages of the local values are calculated using numerical blocks with $S_N > 5\%$. This threshold was set based on previous observations for the *Zhang et al*. [2008] simulated experiments showing that organic saturations lower than 5% did not contribute significantly to mass flux compared to higher saturation pools [*Kokkinaki et al*., 2013a]. It is recognized that this threshold may vary depending on the source zone architecture and the numerical discretization of the model. Physically speaking, this imposed condition implies that local saturations lower than this threshold would produce a weaker signal than that of pools and would, therefore, not affect the average effluent concentrations measured at monitoring wells.

All three variables are normalized with their initial values, so that they represent changes relative to the initially evaluated condition of the source zone, corresponding to the time $\bar{C}_0$ is measured. Similarly to the ESM model, all three parameters of the PB model need to be updated as the source zone is changing with time, such that changes in the source zone architecture are explicitly considered. In this study, two PB model variants are evaluated: Process-based model 1 (PB1) using equation (7), and Process-based model 2 (PB2) using equation (8). The PB models are compared to the ESM and the DDGTP model using the *Zhang et al*. [2008] experiments, and then the PB and DDGTP models are evaluated using an extended suite of hypothetical source zones. For all upscaled models, input parameters that require source zone information are calculated from the discretized numerical model results.

3. Results

3.1. Validation of the PB Upscaled Model

3.1.1. Experimental Effluent Concentrations and Discretized Numerical Model Performance

Figures 3a and 3b show the initial DNAPL spatial distribution for Experiments 1 and 2 of *Zhang et al*. [2008], as predicted by the numerical simulation with COMPSIM. Both experiments featured a complex DNAPL distribution that resulted in abrupt changes in the extent of the source zone. These abrupt changes led to nonsmooth changes in the flow dynamics of the system and produced multistage behavior in the effluent concentration profiles, similar to that observed in other experimental studies [*Powers et al*., 1998; *Nambi and Powers*, 2000; *DiFilippo et al*., 2010]. As shown in Figures 3c and 3d, the breakthrough curves of both experiments are nontypical in that they do not exhibit the characteristic slow initial decrease associated with DNAPL pools, even though both experiments were pool dominated. Instead, concentrations increase at early times, and exhibit variably decreasing rates thereafter. Analysis of this complex behavior at the local scale in a previous study indicated that the increases in concentrations were a result of decreasing DNAPL saturations and increasing aqueous phase relative permeabilities, which in turn result in faster mass transfer [*Kokkinaki et al*., 2013a]. This mechanism was also found to influence subsequent fluctuations in concentrations, to a degree depending on the changes of the DNAPL spatial extent.

Complex source zone architectures are also likely to result in mass transfer limitations, i.e., concentrations lower than solubility, at the local scale. Such limitations are associated with low velocities or low interfacial areas and will also affect the cumulative mass discharge observed at downgradient locations. This was the case for Experiments 1 and 2, as numerical simulations assuming equilibrium dissolution overpredicted the observed effluent concentrations [*Kokkinaki et al*., 2013a]. In contrast, concentrations were effectively captured when local dissolution was modeled using a thermodynamic dissolution model that explicitly accounts for the local effects of velocities and DNAPL-water interfacial areas [*Grant and Gerhard*, 2007; *Kokkinaki et al*., 2013a]. Predictions given by this model are shown in Figures 3c and 3d. Significant advantages of using the thermodynamic dissolution model for the numerical simulations in this study are that it has been validated, and that it only requires knowledge of soil properties and DNAPL distribution to capture mass transfer limitations. As such, it can be used to give reliable estimates of effluent concentrations for hypothetical domains and arbitrarily complex source zones, without neglecting the possible impacts of mass transfer limitations. Therefore, the results of the comprehensive discretized REV-scale numerical model used in this study provide an appropriate validation data set for the evaluation of the upscaled models.

The multistage concentration profiles of the two experiments provide characteristic examples of source zones that cannot be described by simple exponentially decreasing functions, like those of power law upscaled models. Power law models, because of their conceptual simplicity, have been incorporated in several screening tools often used by practitioners, like BIOSCREEN and REMCHLOR [U.S. EPA, 1996; *Falta et al*., 2008; NRC, 2004]. It has also been suggested that power law models can be further simplified by assuming that the exponent is equal to 1 [*Falta et al*., 2005a; *Newell et al*., 2006; *McGuire et al*., 2006; *Fure et al*., 2006; *Falta et al*., 2008]. Figure 4 shows the concentration reduction—mass reduction curves for Experiments 1 and 2. Concentration reductions (black lines) become negative at first, and, then, they exhibit a similar variability in slopes as the normalized concentrations. For comparison purposes, power law functions are also shown for three different exponents. It can be readily seen, that no single value can reproduce the observed variability, while the negative concentration reductions would not be captured, even if the exponent was varied. Moreover, if the exponent was calibrated to a subset of the concentration data, using the calibrated value to predict future concentrations would not have captured the observed changes in concentrations. These changes in concentrations are associated with the changing source zone architecture, which is further explored in the next section.

3.1.2. Source Zone Architecture Metrics

The spatial characteristics of the two source zones were evaluated in time, in order to explore potential correlations with flux-averaged effluent concentrations. The first metric evaluated was the ganglia fraction (GF). The GF is the well-known ganglia-to-pool ratio expressed in a percentage form, and defined as $GF = GTP/(1+GTP)$. The GTP is calculated here on a volume basis, similar to previous studies [*Christ et al*., 2006; *Lemke and Abriola*, 2006]:

$$GTP = \frac{\sum S_N \forall S_N < S_{N,thres}}{\sum S_N \forall S_N \geq S_{N,thres}} \tag{16}$$

The maximum residual organic saturation for the soil types used in the experiments is used here as the upper threshold saturation for the calculation of GF $(S_{N,thres} = 0.15)$, consistent with previous studies [*Christ et al*., 2006]. The GTP has been previously linked to the behavior of flux-averaged effluent concentrations [*Lemke and Abriola*, 2006; *Suchomel and Pennell*, 2006; *Christ et al*., 2006, 2010] and has been proposed as an important metric for DNAPL remediation in regulatory guidance [*ITRC*, 2005; *SERDP*, 2006].

Figures 5a and 5b illustrate the GF with time for Experiments 1 and 2, respectively. Experiment 1 had more ganglia than Experiment 2, and both source zones exhibited a $GF < 0.75$ until late times, such that both source zones can be characterized as pool dominated, following the definition of *Christ et al*. [2010]. Previous studies have suggested that the evolution of *GF* in time may be linked with concentration fluctuations [*DiFilippo and Brusseau*, 2011]. Here, for both experiments, *GF* remains relatively constant until later times. It is also noteworthy that for both experiments the GF increases as dissolution progresses, a behavior likely to be encountered in pool-dominated source zones, as opposed to source zones with higher initial GF [e.g., *Suchomel and Pennell*, 2006; *Christ et al*., 2006].

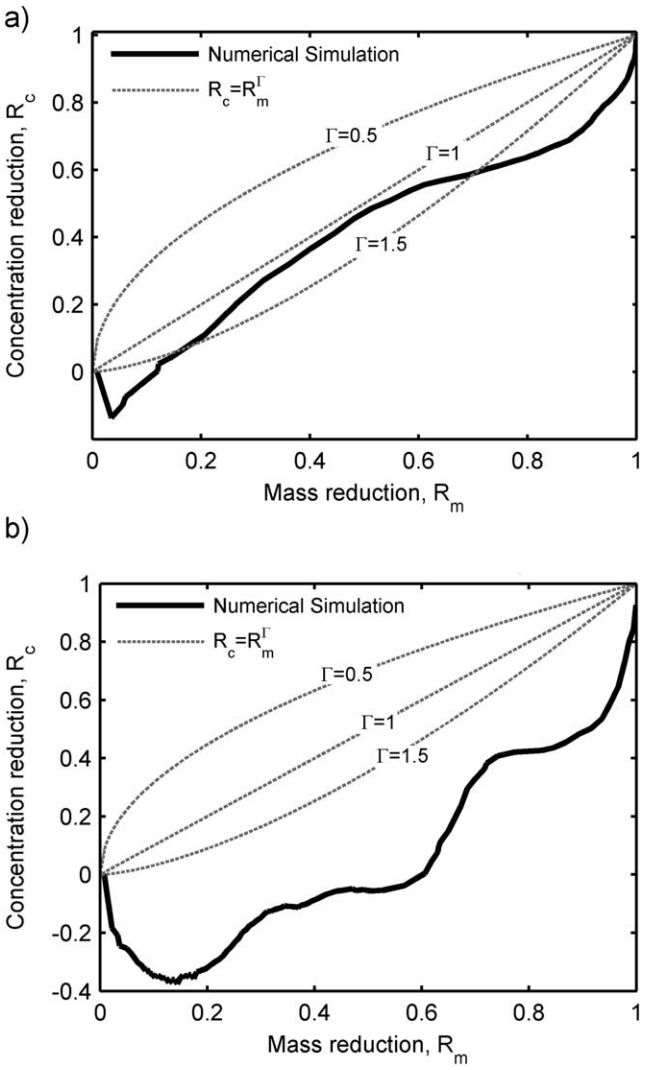

Figure 4. Concentration reduction (R_c) versus mass reduction (R_m) curves for (a) Experiment 1 and (b) Experiment 2.

Figures 5c and 5d show the second spatial moments (M_{II}) of the source zone with time in each of the *x*, *y*, and *z* directions. The spatial moments are decreasing in time as the source zone is shrinking due to dissolution, with the longitudinal and vertical spread decreasing the fastest. Here both experiments show a rather steady decrease in M_{II}, without major fluctuations in slope. Also related to the source zone spread is the term A_{yz}, which is shown in Figures 5e and 5f. A_{yz} is equal to the proportion of the control plane directly downgradient of DNAPLs. Similar to $M_{II,z}$, A_{yz} is decreasing with time, due to the reduction of the source zone size with dissolution. The changes in the reduction rate of A_{yz} reflect the complex distribution of the DNAPL source zone. Slow drops indicate the prevalence of source zone areas where the DNAPL longitudinal extent was thicker, and, therefore, took longer to dissolve, and conversely, fast drops correspond to areas with a smaller amount of DNAPL that dissolved quickly. While the evolution of A_{yz} is similar to that of M_{II}, the spatial moments show smoother temporal changes as they represent weighted averages of saturations. This difference has important implications for the performance of the ESM and PB models, as discussed later in this section.

3.1.3. Upscaled Predictions of the Zhang et al. [2008] Experiments

The upscaled models are used next to calculate the effluent concentrations of the two *Zhang et al.* [2008] experiments. Input parameters for the upscaled models are calculated from the fine-scale numerical simulation with COMPSIM. Figure 6 shows predictions from the numerical simulation together with the predictions of five upscaled models: the DDGTP model, the original ESM model, a calibrated ESM model, the PB1 model, and the PB2 model.

The DDGTP model did not capture the trends in concentrations for either experiment. Although it predicted a multistage behavior for Experiment 1, the second stage started at a very low mass reduction. This is because the DDGTP model assumes that the second stage begins at a mass reduction equal to the initial GF, which was ~0.04 and ~0.01 for Experiment 1 and 2, respectively (Figures 5a and 5b). For the second stage, the DDGTP model did not match the rate of decrease in concentrations. Overall, the DDGTP model overpredicted concentrations for Experiment 1 and underpredicted concentrations for Experiment 2, and did not capture the changes in slope for either of the two experiments. The above results illustrate two major limitations of the DDGTP conceptual model: First, based on the definition of the GF, all parts of the source zone are treated equally, i.e., ganglia at the dissolution front are considered equal to ganglia at inaccessible areas within the source zone. As such, the value of the

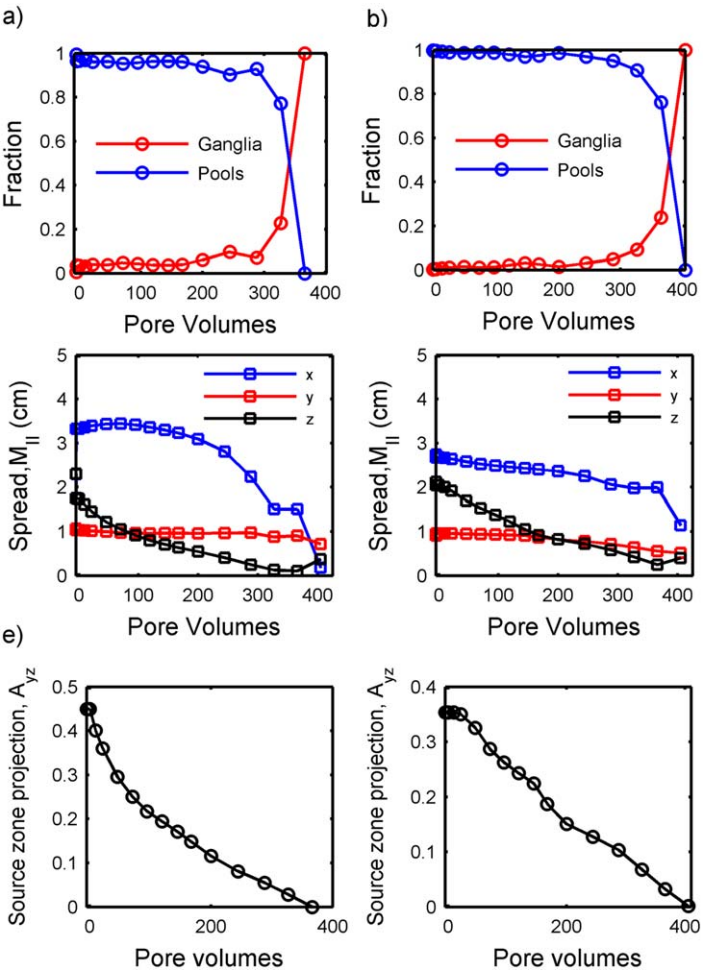

Figure 5. Source zone architecture metrics for (left column) Experiment 1 and (right column) Experiment 2. (a and b) Percentage of DNAPL volume present as ganglia or pools, (c and d) second spatial moment of organic saturation in each direction, and (e and f) projection of the source zone on the control plane.

initial GF is influenced by the presence of ganglia that may not affect mass discharge significantly. Second, all pools are assumed to behave similarly, since the same exponent of 0.5 is used regardless of the pool characteristics. Overall, both exponents used by the DDGTP model to represent each domain are based on empirical observations from a limited set of numerically generated source zones and may not be representative for source zones of more complex characteristics.

The ESM model resulted in a reasonable fit for Experiment 1 when the exponent β was calibrated ($\beta = 0.7$). The good agreement at early times was ensured by the modification of the *Saenton and Illangasekare* [2007] model, such that the constant terms of equation (13) were calculated from $\bar{C}_0$. Temporal changes in the second spatial moment of DNAPL saturations $M_{II,z}$, the only variable parameter of the ESM model, were reflected in the slope change at 58% mass reduction for Experiment 1. However, for Experiment 2, the calibrated ESM model ($\beta = 0.2$) did not predict either the increases in concentrations, or the changes in slopes. Inspection of Figure 5d shows that this is the result of the smooth decrease in $M_{II,z}$, despite the complex distribution of the source zone. As previously noted, spatial moments are weighted averages and, as such, they tend to smooth out effects of local changes. For both experiments, the original exponent $\beta = 4.157$ predicted a near-zero concentration at a 40% mass reduction. This illustrates the importance of calibrating the parameters of empirical models for every different source zone. This additional calibration step, although it may provide better fits, limits the practical utility of the ESM model for upscaling.

Unlike the DDGTP and ESM models, both the PB1 and the PB2 models captured all important features of the two breakthrough curves. To help interpret model results shown in Figure 6, changes in the PB model parameter values are illustrated in Figure 7. For Experiment 1, the change in slope of effluent concentrations at 58% mass removal (120 pore volumes) was predicted by the PB models. This change is concomitant with the decrease in the slope of the A_{yz} curve (Figure 5e) and the sharp increase in average aqueous phase relative permeability $\bar{k}_{w,rel}$ (Figure 7a). The product $\bar{k}_{w,rel} \cdot \bar{S}_N$ shows milder changes with time, due to the decrease in average saturations, and reflects the combined effect of the increasing mass transfer due to increasing flow through the source zone, and the decreasing mass transfer due to lower interfacial areas as dissolution progresses. The significance of the term $\bar{k}_{w,rel} \cdot \bar{S}_N$ is more apparent for Experiment 2, where it led to the increases in predicted concentrations, consistent with the experimental observations (Figure 7b). For Experiment 2, although the PB models overpredicted the magnitude of concentrations, the timing of the slope changes is consistent with the numerical simulation and the experimental data.

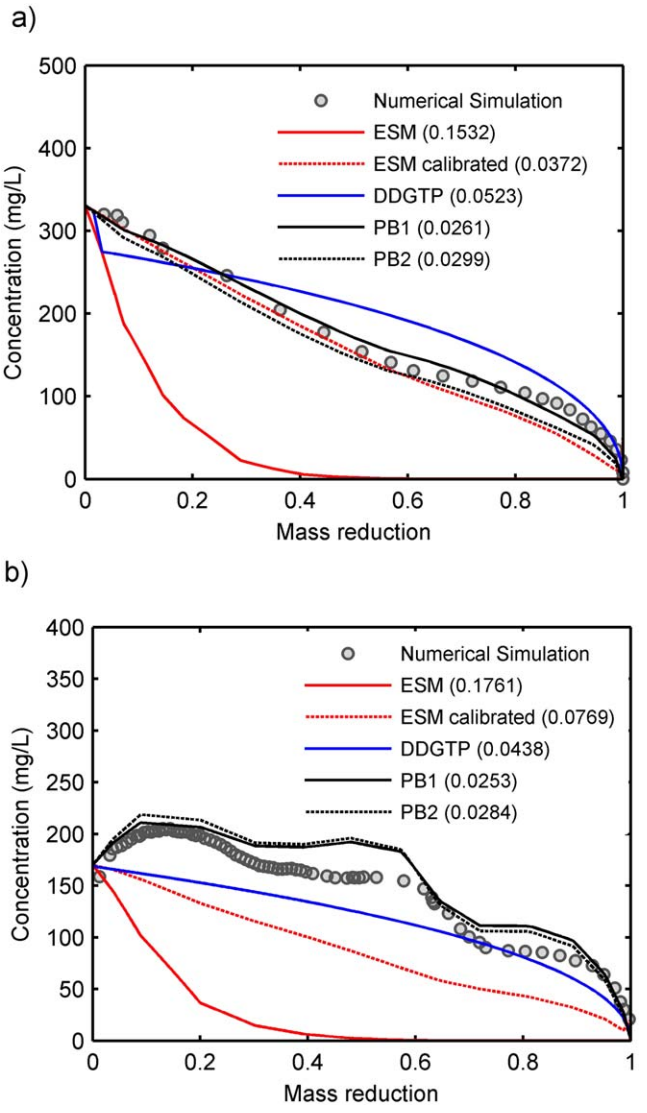

Figure 6. Effluent concentrations predicted by the numerical simulation and the upscaled models for (a) Experiment 1 and (b) Experiment 2. Numbers in parentheses indicate root mean square errors (RMSEs).

Overall, the PB models describe the concentrations for the two DNAPL source zones well, capturing their nonmonotonic, multistage behavior, as well as the timing and extent of changes in concentrations. The average goodness of fit for the PB models compared to the alternative upscaled models is better, as indicated by the lower root mean square error (RMSE) values. Comparing the two PB models, both PB1 (equation (7)) and PB2 (equation (8)) resulted in similar concentrations, due to the low initial concentrations of the two experiments which results in equation (7) to converge to equation (8). Source zones where this condition does not hold are evaluated next to better delineate the differences between the two PB upscaled models.

3.2. Extended Evaluation of the PB Upscaled Models

To further investigate whether the variations in the three parameters, A_{yz}, $\bar{k}_{w,rel}$, and $\bar{S}_N$ of the PB upscaled models are responsible for multistage changes in concentrations, and a series of additional hypothetical simulations were conducted to obtain a wider range of source zone architectures. Models PB1 and PB2 were compared to the DDGTP model. Since our objective in this evaluation is to identify the source zone characteristics that explain concentration variations without having to calibrate empirical parameters, the ESM model was not included in this evaluation. For the comparison, 12 different cases (A through L) were considered, each different from the *Zhang et al*. [2008] experiments in a single attribute. A summary of the 12 cases is given in Table 1. Results for Cases A through F are presented in Figure 8 and discussed below, and results and discussion for Cases G through L are provided in the supporting information. The agreement between the upscaled models and the numerical model is evaluated using root mean square errors (RMSEs) for the average goodness of fit, as well as visual observation for the match in the critical features of concentration profiles like the timing of changes in slope.

Cases A and B evaluated the upscaled models for different flow and mass transfer dynamics, as affected by the hydraulic gradient. Experiment 1 was simulated with a 50% lower hydraulic gradient (Case A) and a 50% higher hydraulic gradient (Case B). This resulted in an average Darcy velocity of 0.5 and 1.5 m/d, respectively. This change did not have an impact on the initial source zone architecture, as it was only implemented during the flushing period of the experiments. However, since velocity is positively correlated with local mass transfer coefficients [*Pfannkuch*, 1984; *Powers et al*., 1994], higher velocities result in faster

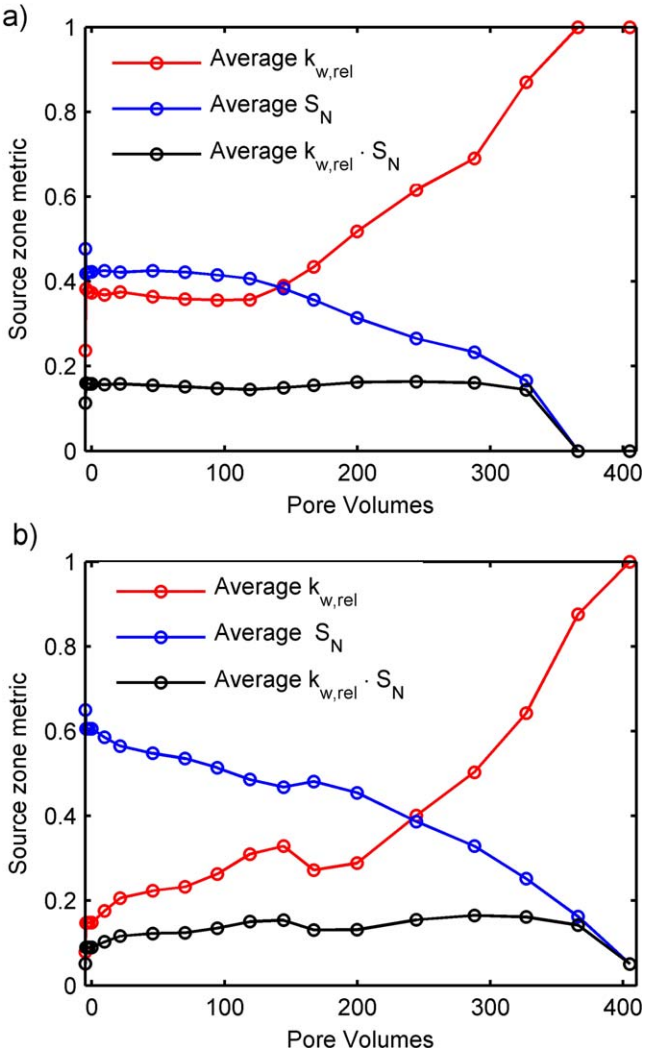

Figure 7. Source zone parameters used in the upscaled PB model for (a) Experiment 1 and (b) Experiment 2.

mass transfer, higher effluent concentrations, and faster mass depletion. At the same time, higher velocities result in smaller retention times and potentially mass transfer limitations. These effects are taken into account by the numerical simulations, shown as gray circles in Figure 8. In contrast, upscaled models only consider upscaled, domain-averaged source zone characteristics. Ideally, these upscaled characteristics should implicitly include the effects of local-scale phenomena (e.g., mass transfer limitations) so that the respective upscaled models can capture the average effluent concentrations.

For both cases A and B, the DDGTP model predicted a two-stage concentration profile similar to that of Experiment 1, since the initial source zone architecture (and the GF_0) did not change (Figures 8a and 8b), and concentration changes were not captured in either of the two cases. Both PB models better matched the decrease in concentrations for Case A with similar RMSEs, slightly underestimating concentrations at high mass reductions. Note that concentrations in Figure 8 are normalized with the initial concentration, such that the smaller the initial concentration (e.g., Case A), the smaller the actual error. For Case B, only model PB2 matched the concentrations well, resulting in the lowest RMSE. Model PB1 predicted the timing of the major changes in slope correctly, but overpredicted the concentrations and resulted in an RMSE similar to that of the DDGTP model. This is contrary to what was expected: PB2 is an approximation of PB1 and should, therefore, fail when $k_{eff}L/\bar{q}$ (i.e., for higher initial concentrations). The good match given by PB2 indicates that the relative changes in the projected area, relative permeability, and saturation have a direct proportional impact on effluent concentrations, rather than on the effective mass transfer coefficient. This suggests that the proportional conceptual model of PB2 better represents the upscaled DNAPL systems, and that the good fit of PB1 in previous cases is due to the convergence of the two mathematical expressions for low $\bar{C}_0$.

Case C evaluates the upscaled models for a simulation where more pronounced mass transfer limitations, i.e., lower local mass transfer rates, were imposed on the system. For this purpose, instead of using the thermodynamic dissolution model to perform the numerical simulation of Experiment 1, the empirical Sherwood-Gilland correlation of *Powers et al*. [1994] was used. The *Powers et al*. [1994] correlation was developed using column data of styrene dissolution and has been previously shown to underestimate concentrations when applied to the more complex source zone of the *Zhang et al*. [2008] experiments [*Kokkinaki et al*., 2013b]. Although the use of the *Powers et al*. [1994] correlation does not represent the actual experimental conditions, this hypothetical case is used here to demonstrate that the parameters of the proposed

Table 1. Summary of Hypothetical Cases Used to Evaluate the PB and DDGTP Models

Case	Varied Attribute
Variations in Mass Transfer Dynamics	
A	50% lower hydraulic gradient
B	50% higher hydraulic gradient
C	Local mass transfer rate
D	Source zone accessibility
Variations in SZ Architecture	
E	50% less DNAPL (Experiment 1)
F	50% less DNAPL (Experiment 2)
G	Complex, pool dominated
H	Complex, pool dominated
I	Complex, pool dominated
J	Homogeneous, sand 20/30
K	Homogeneous with lense, sand 20/30
L	Homogeneous with lense, sand 30/40

PB upscaled model implicitly take into account potential mass transfer limitations. As such, the PB model can be applied for source zones with or without mass transfer limitations without any modification. As Figure 8c shows, the PB models captured the lower concentrations and the changes in slope with mass removal for the whole duration of the simulation, resulting in both the lowest RMSEs, and better capturing the timing and extent of concentration changes than the DDGTP model. The DDGTP model predicted an early drop in concentrations and overestimated concentrations at later times, similarly to cases A and B. This was expected, as the initial source zone architecture was the same for all three cases.

Case D evaluates the upscaled models for the situation where mass transfer is impeded by limited contact between the DNAPL and flowing groundwater. To generate the source zone architecture that resulted in this effect, the soil type definition of Experiment 1 was modified such that part of the DNAPL infiltrated within a high-permeability lense surrounded by less permeable soil. When only the trapped DNAPL pool remained (at 85% mass reduction), the numerical model predicted concentrations at near-zero values. The upscaled DDGTP model did not predict the sharp decrease in concentrations when the trapped DNAPL remained. In contrast, the PB models matched the sharp decrease in concentrations, because the average relative permeability decreased to close to zero values when the trapped DNAPL pool remained, producing low concentrations even though DNAPL was still present in the system. In addition, the PB models closely captured the subtle changes in curvature of concentrations at all times, while the DDGTP model did not predict the

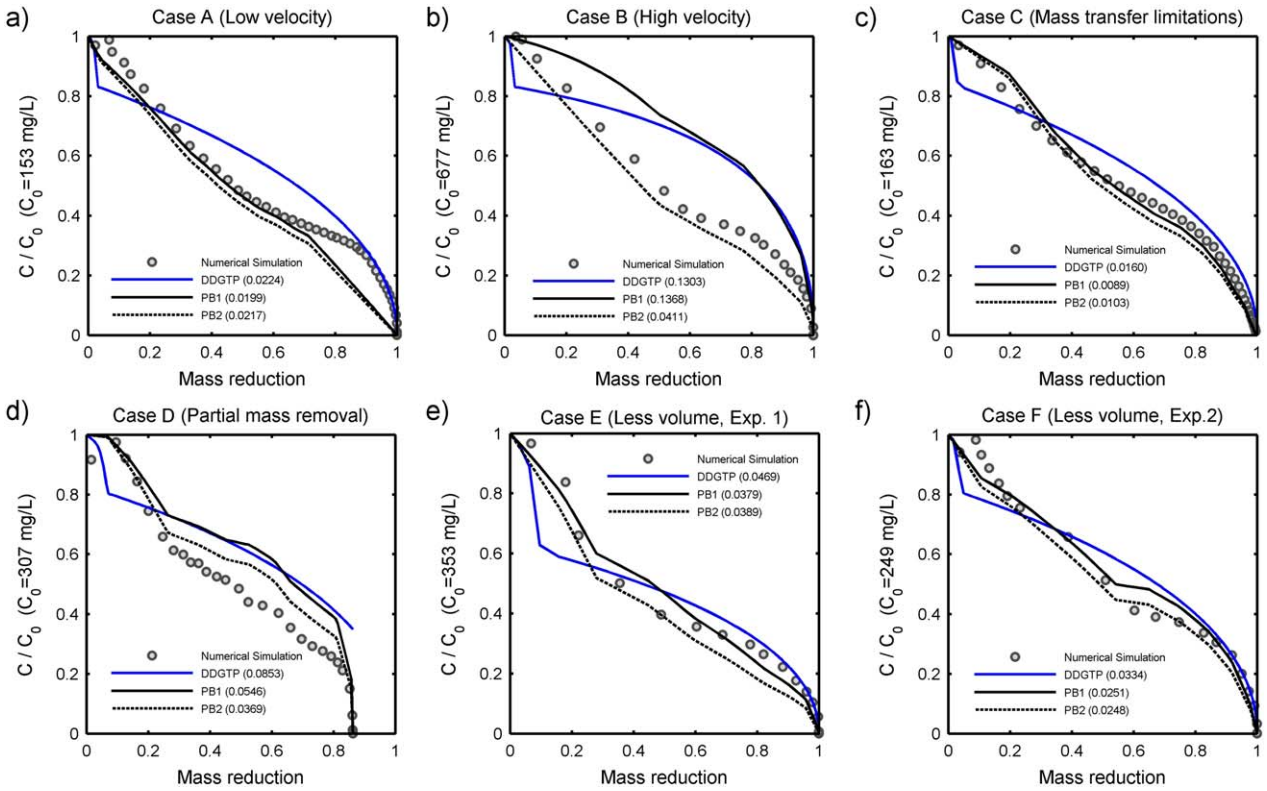

Figure 8. Predicted flux-weighted concentrations as a function of mass removal for cases A–F, for numerical simulations (circles) and upscaled models (lines). Concentrations are normalized with the initial concentration C_0, which is given in parenthesis on the *y* axis for each case. Numbers shown in the legend indicate root mean square errors (RMSEs).

change in slope of the concentrations at earlier times and overpredicted the concentrations for most of the simulation, resulting in the highest RMSE.

Cases A-D were similar in terms of the temporal evolution of ganglia fractions, which were less than 10% and only exceeded 20% near complete depletion of the DNAPL. Additional simulations (Cases E-L) were conducted to evaluate the ability of the upscaled models to predict concentrations for source zones with a more diverse distribution of saturations.

Cases E and F correspond to Experiments 1 and 2, respectively, with 50% less DNAPL injected (11.3 mL). This resulted in smaller source zones, more flow bypassing and dilution, higher ganglia fractions, and less complex and extensive DNAPL pools. These changes were reflected in earlier and milder concentration reductions compared to the real experiments. In both cases, the PB models captured the concentrations and the respective changes in slopes equally well, with similar RMSEs that were lower than those of the DDGTP model. The DDGTP model predicted a clear multistage concentration for case E, due to the higher initial ganglia fraction, however, it still predicted an earlier decrease in concentrations for both cases E and F, and, therefore, underpredicted the concentrations at low mass reductions.

Cases G through L are presented in the supporting information. These cases evaluated source zones architectures that were entirely different from these of Experiments 1 and 2, with a wider range of distributions and ganglia fractions. These different DNAPL distributions resulted in significantly different concentrations profiles (Figure S1, supporting information). In all six cases, model PB2 captured the variations in concentrations better than the PB1 and the DDGTP models in terms the average goodness of fit. An exception is Case I, where the average error (RMSE) of the PB models was higher than that of the DDGTP model; notably, the PB models better matched the timing of concentration changes and the overall shape of the concentration profile.

Overall, the PB models successfully captured the number and timing of the different stages for all source zones evaluated, confirming that the three PB upscaled parameters had a direct influence on the average effluent concentrations. Model PB1 overpredicted the concentrations in cases H, J, and K, which had higher initial concentrations, while in cases with low initial concentrations it gave similar results to PB2. This suggests that a simple proportional conceptual model (equation (8)) better represents the evaluated upscaled DNAPL systems than the one-dimensional effective mass transfer model (equations (3), (4), and (7)). Finally, the DDGTP model did not accurately predict the concentration fluctuations in any of the cases considered here, as all source zones evaluated were pool dominated initially and, therefore, did not adhere to the dual-domain hypothesis. The performance of the DDGTP model did not improve when the actual changes in PF with time were considered instead of using equation (12).

These results indicate that multistage mass discharge from DNAPL source zones may not be related to transitions from ganglia-dominated to pool-dominated source zones, but rather to changes in the overall source zone extent, and in the average flow dynamics within the DNAPL source zone, represented by changes in the average water relative permeability and organic saturation. The importance of these three macroscopic parameters included in the PB models is consistent with previous studies indicating that heterogeneity in the DNAPL saturation and velocity distribution is linked to abrupt reductions in concentrations [*Rao and Jawitz*, 2003]. The results presented here provide a better physical understanding of this link and suggest that conditions under which the commonly used power law models are not representative would be often encountered in complex source zones. This information is important to consider when utilizing existing screening models for DNAPL remediation. Most importantly, these findings can be useful in the development of new nonempirical predictive upscaled models that are more reliable and better suited for implementation within flexible, integrated DNAPL site strategies suggested by current regulatory guidance [*SERDP*, 2006; *ITRC*, 2011].

4. Conclusions

DNAPL source zones often have complex architectures that are difficult to characterize in detail in the field. While numerous studies have shown that the dissolution, and thereby the remediation potential, of DNAPL

source zones is sensitive to this architecture, it is unclear to date which spatial characteristics are most important. Such knowledge would be invaluable in the field, where application of detailed multiphase numerical models is not feasible. The objective of this work was to identify macroscopic characteristics of DNAPL source zones that control average effluent concentrations and to develop an upscaled model describing the relationship between these source zone characteristics and effluent concentrations as both evolve in time. Specific focus was given on effluent concentration profiles that exhibit complex, multistage, nonmonotonic behavior.

Our analysis considers three macroscopic characteristics of the DNAPL source zone: (a) the projected area of the source zone on a downgradient control plane, (b) the average of local-scale aqueous phase relative permeabilities in the source zone, and (c) the average of local-scale DNAPL saturations in the source zone. These three macroscopic parameters represent the cumulative effects of the physical processes affecting downgradient concentrations, namely effluent dilution and local dissolution kinetics. Using fine-scale numerical modeling data for both real and hypothetical centimeter-scale source zones with complex architectures as a validation data set, it was found that a simple proportional relationship between effluent concentrations and the product of the three macroscopic parameters successfully described the behavior of all sixteen source zones evaluated. This indicates that the three transient parameters of the PB model are sufficient for describing the temporal evolution of effluent concentrations. This proposed process-based model (PB model) better matched the concentration profiles of the cases evaluated than an empirical power law upscaled model (ESM model) and a dual-domain ganglia-to-pool ratio model (DDGTP model).

These findings provide a quantitative explanation for the nonmonotonic, multistage concentration profiles often observed for complex DNAPL source zones. The proposed relationship between average effluent concentrations and the source zone macroscopic characteristics can be used to associate observed temporal changes in concentrations with the temporal evolution of the source zone characteristics, such as for example, a decrease in the cross-sectional area of the source zone. Knowledge of such information can lead to better management of remediation operations, by identifying which parameters are important to reassess through the course of remediation and when to do so, and could be applied at sites implementing the current guidance for integrated DNAPL site strategies.

Currently, the three macroscopic parameters of the PB model, namely the projection of the source zone on the control plane and the averages of local DNAPL saturations and water relative permeabilities, are difficult to measure in the field. However, with advances in source zone characterization techniques, such field measurements may become feasible in the near future [e.g., *Annable et al*., 1998; *Jawitz et al*., 2003; *Li and Abriola*, 2009] and may be easier to obtain than more detailed spatial metrics such as the ganglia-to-pool ratio. Also, further model reduction may be possible, due to the relationship between local DNAPL saturations and relative permeabilities. Our results suggest that developing methods to measure or estimate the proposed source zone parameters can be useful for evaluating the potential for significant concentration reductions and the overall longevity of DNAPL source zones.

In conclusion, our analysis of a number of source zone architectures indicates that the temporal evolution of concentrations emanating from complex DNAPL source zones will often not follow the simple exponential-like decrease with mass reduction that is assumed in current state-of-practice screening models. These empirical models, in addition to not capturing complex dissolution behavior, are case specific, requiring calibration of nonphysical parameters for each site at which they are applied. Relationships with parameters directly related to physical characteristics of the source zone like the relationship proposed in this work improve our understanding of how observed reductions in concentrations can be related to changes in source zone DNAPL architecture, information that is important for risk reduction performance evaluation. Improvements in characterization techniques for measuring the proposed macroscopic parameters in the field, combined with methods to predict their temporal evolution would lead to the development of reliable predictive screening for DNAPL site remediation. In those cases where the relative importance of estimating the proposed macroscopic parameters in light of need and availability of resources for obtaining other field data is low, the proposed relationship can be useful in the interpretation of concentration data from monitoring wells.

Acknowledgments
This research was financially supported by the Natural Sciences and Engineering Research Council (NSERC) of Canada, as well as an Ontario Graduate Scholarship (OGS) for the first author. Financial support was also provided by the Ontario Research Fund Research Excellence Water Round Program (Innovative Combined Treatment Technologies for Remediating Contaminated Groundwater Project). We would also like to thank the editor, associate editor, and the three anonymous reviewers for their insightful comments and suggestions on improving our manuscript.

References

Annable, M. D., P. S. C. Rao, K. Hatfield, W. D. Graham, A. L. Wood, and C. G. Enfield (1998), Partitioning tracers for measuring residual NAPL: Field-scale test results, *J. Environ. Eng.*, *124*, 901–908.

Basu, N. B., A. D. Fure, and J. W. Jawitz (2008a), Predicting dense nonaqueous phase liquid dissolution using a simplified source depletion model parameterized with partitioning tracers, *Water Resour. Res.*, *44*, W07414, doi:10.1029/2007WR006008.

Basu, N. B., A. D. Fure, and J. W. Jawitz (2008b), Simplified contaminant source depletion models as analogs of multiphase simulators, *J. Contam. Hydrol.*, *97*, 87–99.

Brusseau, M., N. Nelson, Z. Zhang, J. Blue, J. Rohrer, and T. Allen (2007), Source-zone characterization of a chlorinated-solvent contaminated Superfund site in Tucson, AZ, *J. Contam. Hydrol.*, *90*(1-2), 21–40.

Christ, J. A., C. A. Ramsburg, K. D. Pennell, and L. M. Abriola (2006), Estimating mass discharge from dense nonaqueous phase liquid source zones using upscaled mass transfer coefficients: An evaluation using multiphase numerical simulations, *Water Resour. Res.*, *42*, W11420, doi:10.1029/2006WR004886.

Christ, J. A., C. A. Ramsburg, K. D. Pennell, and L. M. Abriola (2010), Predicting DNAPL mass discharge from pool-dominated source zones, *J. Contam. Hydrol.*, *114*, 18–34.

DiFilippo, E. L., and M. L. Brusseau (2011), Assessement of a simple function to evaluate the relationship between mass flux and mass removal for organic liquid contaminated source zones, *J. Contam. Hydrol.*, *123*(3-4), 104–113.

DiFilippo, E. L., K. C. Carroll, and M. Brusseau (2010), Impact of organic-liquid distribution and flow field heterogeneity on reductions in mass flux, *J. Contam. Hydrol.*, *115*, 14–25.

Dobson, R., M. H. Schroth, M. Oostrom, and J. Zeyer (2006), Determination of NAPL-water interfacial areas in well-characterized porous media, *Environ. Sci. Technol.*, *40*, 815–822.

Falta, R. W. (2008), Methodology for comparing source and plume remediation alternatives, *Ground Water*, *46*(2), 272–285.

Falta, R. W., P. Suresh Rao, and N. Basu (2005a), Assessing the impacts of partial mass depletion in DNAPL source zones: I. Analytical modeling of source strength functions and plume response, *J. Contam. Hydrol.*, *78*(4), 259–280.

Falta, R. W., N. Basu, and P. S. Rao (2005b), Assessing impacts of partial mass depletion in DNAPL source zones: II. Coupling source strength functions to plume evolution, *J. Contam. Hydrol.*, *79*(1-2), 45–66.

Fure, A. D., J. W. Jawitz, and M. D. Annable (2006), DNAPL source depletion: Linking architecture and flux response, *J. Contam. Hydrol.*, *85*, 118–140.

Gerhard, J. I., and B. Kueper (2003a), Capillary pressure characteristics necessary for simulating DNAPL infiltration, redistribution and immobilization in saturated porous media, *Water Resour. Res.*, *39*(8), 1212, doi:10.1029/2002WR001270.

Gerhard, J. I., and B. Kueper (2003b), Influence of constitutive model parameters on the predicted migration of DNAPL in heterogeneous porous media, *Water Resour. Res.*, *39*(10), 1279, doi:10.1029/2002WR001570.

Gerhard, J. I., and B. Kueper (2003c), Relative permeability characteristics necessary for simulating DNAPL infiltration, redistribution and immobilization in saturated porous media, *Water Resour. Res.*, *39*(8), 1213, doi:10.1029/2002WR001490.

Grant, G. P., and J. I. Gerhard (2007), Simulating the dissolution of a complex DNAPL source zone: 2. Experimental validation of an interfacial area-based mass transfer model, *Water Resour. Res.*, *43*, W12409, doi:10.1029/2007WR006039.

ITRC (2004), Strategies for monitoring the performance of DNAPL source zone remedies, in *Technical Regulatory Guidance*, Dense Nonaqueous Phase Liquids Team, Interstate Technol. and Regul. Counc., Washington, D.C.

ITRC (2005), Overview of in situ bioremediation of chlorinated ethene DNAPL source zones, in *Technical Regulatory Guidance*, Bioremediation of DNAPLs Team, Interstate Technol. and Regul. Counc., Washington, D.C.

ITRC (2010), Use and measurement of mass flux and mass discharge, in *Technical Regulatory Guidance*, Integrated DNAPL site strategy Team, Interstate Technol. and Regul. Counc., Washington, D.C.

ITRC (2011), Integrated DNAPL site strategy, in *Technical Regulatory Guidance*, Integrated DNAPL site strategy Team, Interstate Technol. and Regul. Counc., Washington, D.C.

Jawitz, J. W., M. D. Annable, G. G. Demmy, and P. S. C. Rao (2003), Estimating nonaqueous phase liquid spatial variability using partitioning tracer higher temporal moments, *Water Resour. Res.*, *39*(7), 1192, doi:10.1029/2002WR001309.

Jawitz, J. W., A. D. Fure, G. G. Demmy, S. Berglund, and P. S. Rao (2005), Groundwater contaminant flux reduction resulting from nonaqueous phase liquid mass reduction, *Water Resour. Res.*, *41*, W10408, doi:10.1029/2004WR003825.

Kokkinaki, A., D. O'Carroll, C. J. Werth, and B. E. Sleep (2013a), Coupled simulation of DNAPL infiltration and dissolution in three dimensional heterogeneous domains: Process model validation, *Water Resour. Res.*, *49*, 7023–7036, doi:10.1002/wrcr.20503.

Kokkinaki, A., D. O'Carroll, C. J. Werth, and B. E. Sleep (2013b), An evaluation of Sherwood-Gilland correlations for NAPL dissolution and their relationship to soil properties, *J. Contam. Hydrol.*, *155*, 87–98.

Kueper, B. H., W. Abbott, and G. Farquhar (1989), Experimental observations of multiphase flow in heterogeneous porous media, *J. Contam. Hydrol.*, *5*, 83–95.

Lemke, L. D., and L. M. Abriola (2006), Modeling dense nonaqueous phase liquid mass removal in nonuniform formation: Linking source zone architecture and system response, *Geosphere*, *2*(2), 74–82.

Li, K. B., and L. M. Abriola (2009), A multistage multicriteria spatial sampling strategy for estimating contaminant mass discharge and its uncertainty, *Water Resour. Res.*, *45*, W06407, doi:10.1029/2008WR007362.

McClure, P., and B. Sleep (1996), Simulation of bioventing for soil and ground-water remediation, *J. Environ. Eng.*, *122*, 1003–1011.

McGuire, T. M., J. M. McDade, and C. J. Newell (2006), Performance of DNAPL source depletion technologies at 59 chlorinated solvent-impacted sites, *Ground Water Monit. Rem.*, *26*(1), 73–84.

Nambi, I. M., and S. E. Powers (2000), NAPL dissolution in heterogeneous systems: An experimental investigation in a simple heterogeneous system, *J. Contam. Hydrol.*, *44*, 161–184.

Nambi, I. M., and S. E. Powers (2003), Mass transfer correlations for nonaqueous phase liquid dissolution from regions with high initial saturations, *Water Resour. Res.*, *39*(2), 1030, doi:10.1029/2001WR000667.

Newell, C. J., I. Cowie, T. M. McGuire, and W. W. McNab Jr. (2006), Multi-year temporal changes in chlorinated solvent concentrations at 23 monitored natural attenuation sites, *J. Environ. Eng.*, *132*, 653–663.

NRC (2004), Source remediation technology options, in: Contaminants in the Subsurface: Source Zone Assessment and Remediation, pp. 178-305, Committee on Source Removal of Contaminants in the Subsurface, Available at http://www.nap.edu/openbook.php?record_id=11146.

O'Carroll, D., and B. E. Sleep (2007), Hot water flushing for immiscible displacement of a viscous NAPL, *J. Contam. Hydrol.*, *91*, 247–266.

O'Carroll, D., and B. Sleep (2009), Role of NAPL thermal properties in the effectiveness of hot water flooding, *Transp. Porous Media*, *79*, 393–405.

Parker, J. C., and E. Park (2004), Modeling field-scale dense nonaqueous phase liquid dissolution kinetics in heterogeneous aquifers, *Water Resour. Res.*, *40*, W05109, doi:10.1029/2003WR002807.

Pfannkuch, H. (1984), Determination of the contaminant source strength from mass exchange processes at the petroleum groundwater interface in shallow aquifer systems, in *Petroleum Hydrocarbons and Organic Chemicals in Ground Water*, pp. 444–458, Natl. Water Well Assoc., Worthington, Ohio.

Powers, S. E., L. M. Abriola, and W. Weber (1994), An experimental inverstigation of NAPL dissolution in saturated subsurface systems: Transient mass transfer rates, *Water Resour. Res.*, *30*(2), 321–332.

Powers, S. E., I. M. Nambi, and G. W. Curry (1998), Non-aqueous phase liquid dissolution in heterogeneous systems: Mechanisms and a local equilibrium modeling approach, *Water Resour. Res.*, *34*(12), 3293–3302.

Rao, P. S. C., and J. W. Jawitz (2003), Comment on ''Steady state mass transfer from single-component dense nonaqueous phase liquids in uniform flow fields'' by T. C. Sale and D. B. McWhorter, *Water Resour. Res.*, *39*(3), 1068, doi:10.1029/2001WR0005992003.

Rao, P. S. C., J. W. Jawitz, C. G. Enfield, R. W. Falta, M. D. Annable, and A. L. Wood (2002), Technology integration for contaminated site remediation: Cleanup goals and performance criteria. In Groundwater Quality 2001, conference proceedings, Edited by S. Thornton and S. Oswald, Int. Assoc. of Hydrol. Sci. Publ no. 275, pp. 571–578.

Saba, T., and T. Illangasekare (2000), Effect of groundwater flow dimensionality on mass transfer from entrapped nonaqueous phase liquid contaminants, *Water Resour. Res.*, *36*(4), 971–979.

Saenton, S., and T. Illangasekare (2007), Upscaling of mass transfer rate coefficient for the numerical simulation of dense nonaqueous phase liquid dissolution in heterogeneous aquifers, *Water Resour. Res.*, *43*, W02428, doi:10.1029/2005WR004274.

Schroth, M. H., S. J. Ahearn, J. S. Selker, and J. D. Istok (1996), Characterization of miller-similar silica sands for laboratory hydrologic studies, *Soil Sci. Soc. Am. J.*, *60*, 1331–1339.

SERDP (2006), SERDP and ESTCP expert panel workshop on reducing the uncertainty of DNAPL source zone remediation, final report. SERDP & ESTCP, Baltimore, Maryland [Available at http://www.serdp.org/content/download/8238/101224/version/1/file/DNAPLWorkshopReport-2006.pdf.]

Sleep, B., and J. Sykes (1993a), Compositional simulation of groundwater contamination by organic compounds: 1. Model development and verification, *Water Resour. Res.*, *29*(6), 1697–1708.

Sleep, B., and J. Sykes (1993b), Compositional simulation of groundwater contamination by organic compounds: 2. Model applications, *Water Resour. Res.*, *29*(6), 1709–1718.

Sleep, B. E., L. Sehayek, and C. Chien (2000), A modeling and experimental study of light nonaqueous phase liquid (LNAPL) accumulation in wells and LNAPL recovery from wells, *Water Resour. Res.*, *36*(12), 3535–3545.

Suchomel, E. J., and K. D. Pennell (2006), Reductions in contaminant mass discharge following partial mass removal from DNAPL source zones, *Environ. Sci. Technol.*, *40*(19), 6110–6116.

U.S. EPA (1996), BIOSCREEN, Natural attenuation decision support system, *User's manual Tech. Rep. EPA/600/R-96/087*, U.S. Environ. Prot. Agency, Office of research and development, Washington, D.C.

U.S. EPA (2003), The DNAPL remediation challenge: Is there a case for source depletion?, *Tech. Rep. EPA/600/R-03/143*, Expert Panel on DNAPL Remediation, Cincinnati, Ohio.

Zhang, C., C. J. Werth, and A. G. Webb (2007), Characterization of NAPL source zone architecture and dissolution kinetics in heterogeneous porous media using magnetic resonance imaging, *Environ. Sci. Technol.*, *41*, 3672–3678.

Zhang, C., H. Yoon, C. J. Werth, A. J. Valocchi, N. B. Basu, and J. W. Jawitz (2008), Evaluation of simplified mass transfer models to simulate the impacts of source zone architecture on nonaqueous phase liquid dissolution in heterogeneous porous media, *J. Contam. Hydrol.*, *102*, 49–60.

Zhu, J., and J. Sykes (2004), Simple screening models of DNAPL dissolution in the subsurface, *J. Contam. Hydrol.*, *72*, 245–258.